Title: A conserved membrane protein negatively regulates Mce1 complexes in mycobacteria

Authors: Yushu Chen[1], Yuchun Wang[1], Shu-Sin Chng[1,2]*

Affiliations:

[1] Department of Chemistry, National University of Singapore, Singapore 117543.

[2] Singapore Center for Environmental Life Sciences Engineering, National University of Singapore (SCELSE-NUS), Singapore 117456.

* To whom correspondence should be addressed. Email: chmchngs@nus.edu.sg

Abstract

Tuberculosis continues to pose a serious threat to global health. *Mycobacterium tuberculosis*, the causative agent of tuberculosis, is an intracellular pathogen that relies on various mechanisms to survive and persist within the host. Among their many virulence factors, mycobacteria encode Mce systems. Some of these systems are implicated in lipid uptake, but the molecular basis for Mce function(s) is poorly understood. To gain insights into the composition and architecture of Mce systems, we characterized the putative Mce1 complex involved in fatty acid transport. We show that the Mce1 system in *Mycobacterium smegmatis* comprises a canonical ATP-binding cassette transporter, associated with functionally redundant heterohexameric assemblies of substrate-binding proteins. Furthermore, we establish that the conserved membrane protein Mce1N negatively regulates Mce1 function via a unique mechanism involving blocking transporter assembly. Our work offers molecular understanding of Mce complexes, sheds light on mycobacterial lipid metabolism and its regulation, and informs future anti-mycobacterial strategies.

Introduction

Tuberculosis (TB) has been one of the top killers among single infectious diseases in humans, alone claiming 1.4 million lives out of 10.6 million new cases in 2021[1]. Apart from the active cases, it is estimated that one quarter of the world population have latent TB, which may progress into active infections[2]. TB is primarily caused by *Mycobacterium tuberculosis*, an organism known for its ability to adapt to the host environment and modulate the host immune system[3]. Its success as a pathogen can be owed to diverse virulence factors encoded in the genome of *M. tuberculosis*. In particular, many of these virulence factors promote host adaptation by contributing to the acquisition and catabolism of important nutrients, including metals, sugars and lipids[4].

mce operons were initially recognized as virulence factors in *M. tuberculosis*[5] and later found to be widespread throughout the *Mycobacterium* genus[6]. *M. tuberculosis* contains four *mce* operons, individually important determinants of virulence and collectively critical for pathogenesis[7–10]. *Mycobacterium smegmatis*, an environmental microorganism, contains six *mce* operons, while *Mycobacterium leprae*, the causative agent of leprosy, has only one such operon (*mce1*) in its highly degenerate genome[6]. In general, an *mce* operon consists of eight genes, two *yrbE* (e.g., *yrbE1A*/*B*) and six *mce* genes (e.g., *mce1A–F)*, with different numbers of accessory genes[6] that may be required for function[11,12] (e.g., *mam1A–D* after the *mce1* operon). Furthermore, a gene encoding a transcriptional regulator (e.g., *mce1R*) can be found upstream of some *mce* operons[6,13,14] (Fig. 1a and Supplementary Fig. 1). The *mce1* and *mce4* operons have been implicated in fatty acid and cholesterol uptake, respectively[9,11,15]. Our understanding of how these operons facilitate lipid uptake is limited.

It is believed that *mce* operons encode ATP-binding cassette (ABC) transporters that are analogous to the MlaFEDB complex in Gram-negative bacteria[6,16], which is important for retrograde transport of phospholipids[17,18]. In MlaFEDB, MlaF, MlaE and MlaD represent the nucleotide-binding domains (NBDs), transmembrane domains (TMDs), and substrate-binding proteins (SBPs), respectively[19,20]. In Mce systems, YrbEA/Bs and MceA–Fs would form the corresponding TMDs and SBPs based on homology; here, MceG, a protein not encoded within *mce* operons, is thought to constitute the NBDs that energize all these putative transporters[21,22] (Fig. 1b). MlaD and MceA–F all contain a single mammalian cell entry (MCE) domain. Interestingly, MlaD and other MCE-domain proteins, such as PqiB and YebT/LetB, have been shown to

51 form homohexamers that provide a hydrophobic tunnel each, presumably for lipid substrate
52 transport[19,20,23,24]. The fact that *mce* operons encode six Mce proteins MceA–F hints at the possible
53 formation of heterohexameric MCE assemblies within each putative transporter. Despite similarities to
54 MlaFEDB, however, there has been a lack of biochemical studies on mycobacterial Mce systems, and their
55 exact compositions and overall architectures remain unknown.

56 Here, we biochemically characterized the putative Mce1 complex in *M. smegmatis*. We show that this
57 system is important for fatty acid uptake, akin to the *M. tuberculosis* Mce1 complex[11,15]. We demonstrate
58 that Mce1 is an ABC transporter comprising a core complex of YrbE1A/B-MceG, associated with a likely
59 heterohexamer of Mce1A–F. We reveal that MSMEG_6540 is a functional homolog that can possibly
60 replace Mce1A in the complex, and in fact, contributes more significantly to the fatty acid uptake function
61 of Mce1. Furthermore, we identify MSMEG_0959, herein renamed to Mce1N, as a negative regulator of
62 the Mce1 system; it prevents MceG from associating with the complex via competitive binding to YrbE1B,
63 thereby modulating transport activity. Our work provides critical insights into the architecture, function and
64 regulation of Mce systems in mycobacteria.

65

66 **Results**

67 **Key proteins encoded in the *mce1* operon co-purify as a complex**

68 To probe the composition of the putative Mce1 complex, we expressed His-tagged YrbE1A or YrbE1B
69 in *M. smegmatis* using an integrative plasmid, and conducted affinity purification following cell lysis and
70 detergent extraction from total membranes. This was done in a Δ*mce1R* strain, where the *mce1* operon is
71 presumably up-regulated[13]. We found that His-tagged YrbE1B, but not YrbE1A, pulled down two distinct
72 protein bands at ~45 and ~19 kDa (Fig. 1c). Tandem mass spectrometry (MS/MS) sequencing of the excised
73 bands indicated that they were MceG (39.0 kDa) and a protein of unknown function, MSMEG_0959 (19.1
74 kDa), respectively. We did not observe additional bands corresponding to other expected members of the
75 Mce1 complex, possibly due to low cellular levels, or instability of the complex *ex vivo*. To detect potential
76 low abundance proteins specifically co-purified with His-tagged YrbE1B, we directly subjected entire gel
77 lanes divided into two sections to MS/MS protein identification. Remarkably, this facilitated the detection
78 of all other putative Mce1 components, including YrbE1A and Mce1A–F, similar to a recent report

identifying YrbE4A/B, Mce4A–F and MceG as components of the Mce4 complex[12]. Interestingly, a seventh MCE-domain protein MSMEG_6540[6] was also co-purified with His_6-YrbE1B, while none of the putative Mce-associated membrane proteins (Mam1A–D and OmamA/B[25]) or LucA[11] was identified. Our data suggest that the Mce1 complex likely comprises the core ABC transporter YrbE1A/B-MceG associated with a presumed heterohexamer of MCE-domain proteins.

MSMEG_6540 and Mce1A are redundant components of the Mce1 system

MSMEG_6540 shares 80% primary sequence identity with Mce1A, compared to less than 20% with other MCE-domain proteins in the Mce1 complex and ~25% with MceA proteins in other putative *M. smegmatis* Mce complexes (Supplementary Table 1). Another Mce1A paralog MSMEG_5818[6], which is only 60% identical, was not co-purified with His-tagged YrbE1B (Fig. 1c). This suggests that MSMEG_6540 could be a functional homolog of Mce1A. We also hypothesized that MSMEG_6540 and Mce1A form heterohexamers with Mce1B–F in distinct complexes. To test these ideas, we examined the effects of removing each MCE-domain protein on fatty acid uptake, a key function of the Mce1 complex[11,15]. Deletion of *yrbE1A*/*B* or *mceG*, both of which are expected to abolish Mce1 function, resulted in significantly reduced [^{14}C]-palmitic acid uptake in cells (Fig. 2a and Supplementary Fig. 2). We established that [^{14}C]-palmitic acid uptake was also reduced to the baseline, i.e., at levels of Δ*yrbE1A*/*B* cells, in individual Δ*mce1B*, Δ*mce1C*, Δ*mce1D*, Δ*mce1E* or Δ*mce1F* mutants. The Δ*mce1C* and Δ*mce1D* strains could be complemented by ectopic expression of the deleted gene alone (i.e., no polar effects) (Fig. 2b). The Δ*mce1B*, Δ*mce1E* or Δ*mce1F* mutants could be fully complemented only when the deleted gene was expressed together with downstream genes, but not when the latter alone was expressed (Fig. 2c–e). Therefore, each of Mce1B–F should be present in all Mce1 complexes and required for fatty acid uptake function.

Unexpectedly, removing Mce1A did not abolish, yet somehow gave increased [^{14}C]-palmitic acid uptake (Fig. 2a). In contrast, the uptake was significantly less efficient in cells lacking *MSMEG_6540*, and only further reduced to the baseline in the Δ*mce1A*Δ*6540* double mutant (Fig. 2a). We showed that expressing *mce1A* in the double mutant increased palmitic acid uptake slightly, to levels similar to the Δ*MSMEG_6540* strain, while expressing *MSMEG_6540* brought uptake to levels higher than wild type

107 (WT) cells, akin to the Δ*mce1A* strain (Fig. 2f). Our results indicate that Mce1A and MSMEG_6540 are
108 functionally redundant, with MSMEG_6540 being more efficient in mediating fatty acid uptake. In fact,
109 expressing Mce1A or MSMEG_6540 in WT cells decreased or increased palmitic acid uptake, respectively,
110 in a Mce1-dependent manner (Supplementary Fig. 3). We conclude that Mce1A and MSMEG_6540
111 compete to form distinct heterohexamers together with Mce1B–F, with the latter Mce1 complex playing a
112 more important role in fatty acid uptake in *M. smegmatis*.
113

114 **YrbE1A/B-MceG constitute the core ABC transporter**

115 We attempted but failed to over-express the *mce1* operon along with *mceG* in *E. coli*. Expression levels
116 of Mce1A–F were very low, which precluded purification of any stable Mce1 complex. Instead, we were
117 able to isolate the core ABC transporter when we co-expressed YrbE1A, His-tagged YrbE1B and MceG.
118 This complex eluted as a single peak on size exclusion chromatography (Fig. 3a); we showed that the
119 purified complex exhibits ATP hydrolytic activity (Fig. 3b), implying proper assembly of YrbE1A/B-MceG.
120 Interestingly, we found that His-tagged YrbE1B alone could pull down MceG when co-expressed in *E. coli*.
121 In contrast, His-tagged YrbE1A could only co-purify with MceG in the presence of YrbE1B, indicating that
122 the TMD-NBD interactions are mainly mediated through YrbE1B (Fig. 3c). Consistent with this idea, an
123 AlphaFold2 structural model of the YrbE1A/B-MceG complex[26–28], which resembles the homologous
124 MlaFE structure from Gram-negative bacteria (RMSD = 2.934 Å)[29], presented a smaller buried area
125 between MceG and YrbE1A (699 $Å^2$) compared to YrbE1B (837 $Å^2$) (Supplementary Fig. 4 and Table 2).
126 We conclude that the TMD and NBD proteins of the Mce1 system interact asymmetrically to form a stable
127 functional ABC transporter.
128

129 **MSMEG_0959 is a negative regulator of Mce1**

130 In addition to MceG, MSMEG_0959 was another protein abundantly co-purified with His-tagged
131 YrbE1B expressed in *M. smegmatis*. MSMEG_0959 is a putative conserved membrane protein with
132 unknown function; it contains two predicted transmembrane helices (TM1: W39–G59; TM2: L65–T90)
133 and a C-terminal cytoplasmic domain (S91–P178) (Supplementary Fig. 5a). We initially hypothesized that
134 it might function to stabilize the Mce1 complex, analogous to the role of the cytoplasmic protein MlaB in

135 the Gram-negative MlaFEDB complex[19]. To test this idea, we attempted to isolate a stable complex
136 containing YrbE1A/B, MceG and MSMEG_0959. To our surprise, when these four proteins were co-
137 expressed and purified from *E. coli*, only MSMEG_0959 was co-purified with His-tagged YrbE1B (Fig.
138 4a). We detected much less YrbE1A and essentially no MceG co-purified, suggesting that MSMEG_0959
139 may destabilize the Mce1 complex instead. In support of this notion, when MSMEG_0959 was over-
140 expressed in *M. smegmatis*, much less MceG was co-purified with His-tagged YrbE1B (Fig. 4c). We
141 conclude that MSMEG_0959 may disrupt YrbE1A/B-MceG interactions.

142 Since TMD-NBD interactions within the Mce1 complex is largely mediated through YrbE1B, we
143 presumed that MSMEG_0959 directly interacts with YrbE1B. Indeed, His-tagged YrbE1B alone, but not
144 YrbE1A, pulled down MSMEG_0959 when co-expressed in *E. coli*, consistent with affinity purification
145 results in *M. smegmatis* (Fig. 1c, Supplementary Fig. 6a and b). We generated an AlphaFold2 structural
146 model comprising YrbE1B and MSMEG_0959[26–28], predicting possible interactions between the
147 transmembrane domain of MSMEG_0959 and that of YrbE1B opposite its dimerization surface with
148 YrbE1A (Fig. 4d). To test the validity of this model, we introduced cysteine pairs across potential contact
149 sites in the transmembrane regions of the two proteins, and looked for disulfide bond formation when these
150 variants are expressed in *E. coli*. Five pairs of cysteines at the periplasmic side of the putative interface
151 enabled crosslinking between YrbE1B and MSMEG_0959 (Fig. 5), lending confidence to the predicted
152 interaction mode. The AlphaFold2 model revealed that an unstructured loop in the cytoplasmic domain of
153 MSMEG_0959 may contact a short helix of YrbE1B sitting at the membrane-water boundary. This helix
154 may be a determinant of the interaction between YrbE1B and MSMEG_0959 since the amino acid sequence
155 of this region is very different from that in YrbE1A (Supplementary Fig. 6c and d). Mutating part of this
156 helix (RLVAEIGMGT) to a flexible loop (GGSSG) did not affect the stability of the YrbE1A/B-MceG
157 complex; however, this mutation prevented co-purification of MSMEG_0959 with His-tagged YrbE1B
158 from *E. coli*, at the same time alleviating the destabilizing effect of MSMEG_0959 on YrbE1A/B-MceG
159 interactions (Fig. 4a). Notably, overlay of the models of YrbE1B-MSMEG_0959 and YrbE1A/B-MceG
160 highlighted substantial steric clashes between MceG and the cytoplasmic domain of MSMEG_0959 (Fig.
161 4d), indicating that their respective interactions with YrbE1B are likely competitive and mutually exclusive.
162 We also generated an MSMEG_0959 variant ($MSMEG_0959_{AGG3P}$) where the cytoplasmic loop that

163 appears to interact with YrbE1B is modified (^{131}ALGELTG to PLPELTP) to impact overall conformation.
164 Intriguingly, this variant still interacts with YrbE1B but is no longer able to compete out MceG when co-
165 expressed in either *E. coli* (Fig. 4b) or *M. smegmatis* (Fig. 4c). Taken together, our results establish that
166 MSMEG_0959 specifically binds YrbE1B and prevents association of the NBD (MceG) to this ABC
167 transporter.

168 Our biochemical experiments suggest that MSMEG_0959 may be a negative regulator of the Mce1
169 complex. Consistent with this idea, MSMEG_0959 over-expression inhibited [^{14}C]-palmitic acid uptake in
170 WT cells, but not residual uptake observed in Δ*yrbE1A*/*B* cells (Fig. 4e). In contrast, over-expression of
171 MSMEG_0959$_{AGG3P}$ did not inhibit [^{14}C]-palmitic acid uptake at all (Fig. 4e), in line with its inability to
172 displace MceG (Fig. 4c). Furthermore, we found that over-expression of Rv0513, the *M. tuberculosis*
173 homolog of MSMEG_0959, reduced the amount of MceG associated with YrbE1B (Fig. 4c) in *M.*
174 *smegmatis*, and slowed down [^{14}C]-palmitic acid uptake (Fig. 4e). We therefore conclude that
175 MSMEG_0959/Rv0513, herein renamed to Mce1N (Mce1 negative regulator), inhibits the fatty acid uptake
176 function of the Mce1 transporter(s) via a conserved mechanism that involves prevention of YrbE1B-MceG
177 interaction.

178

179 **Discussion**

180 In this study, we set out to characterize the Mce1 complex in *M. smegmatis*. We have shown that the
181 Mce1 complexes likely comprise the core inner membrane ABC transporter YrbE1A/B-MceG, associated
182 with heterohexamers composed of Mce1A–F or MSMEG_6540/Mce1B–F. We have demonstrated that
183 MSMEG_6540 is functionally redundant with Mce1A, and indeed more important in the newly
184 characterized fatty acid uptake function of Mce1 in *M. smegmatis*. Furthermore, we have discovered a
185 negative regulator of the Mce1 complex, Mce1N, which physically hinders the dominant TMD-NBD
186 interaction (i.e., YrbE1B-MceG) in the ABC transporter. Our work provides novel insights into the
187 architecture and regulation of mycobacterial Mce complexes.

188 Based on analogy to other MCE-domain proteins, such as MlaD, PqiB[20] and YebT/LetB[23,24] involved
189 in lipid transport in Gram-negative bacteria (Supplementary Fig. 7a), Mce1A–F and
190 MSMEG_6540/Mce1B–F likely form hexamers. Each of these Mce proteins contains a single MCE domain

191 (like MlaD) and an extended helical domain (like PqiB), followed by the presence of an additional C-
192 terminal domain of varied sizes. According to AlphaFold2 prediction[26,27,30], Mce1A or MSMEG_6540 can
193 indeed form a heterohexamer with Mce1B–F (Supplementary Fig. 7b). In contrast, a homohexameric model
194 of Mce1A alone could not be generated, agreeing with an earlier observation that the MCE domain of *M.*
195 *tuberculosis* Mce1A predominantly forms monomers in solution[31]. In the AlphaFold2 model, the
196 heterohexamer adopts an architecture that comprises a hexameric MCE ring connected to a tube formed by
197 a bundle of helical domains; the C-terminal domains of the six Mce proteins organize to form a possible
198 substrate entry point at the very tip (Supplementary Fig. 7b). A continuous hydrophobic tunnel runs through
199 the entire assembly that likely extends across the periplasm to contact the mycobacterial outer membrane
200 (Fig. 6, Supplementary Fig. 7b and c), consistent with its function in lipid uptake. This predicted model
201 resembles the recently solved cryo-electron microscopy (EM) structure of the Mce1 complex remarkably
202 well[32]. Interestingly, *M. smegmatis* possesses MSMEG_6540 as a functional homolog of Mce1A,
203 highlighting the presence of two variants of Mce1 complexes[6], containing Mce1B–F and either Mce1A or
204 MSMEG_6540 (Fig. 6). In support of this idea, removing any other MCE-domain protein in Mce1, but not
205 Mce1A or MSMEG_6540 alone, completely abolishes function in fatty acid uptake (Fig. 2). Differences
206 between the primary sequences of Mce1A and MSMEG_6540 lie mainly in the extreme C-terminal domain,
207 with differing residues primarily mapped to the substrate entry point in the AlphaFold2 models
208 (Supplementary Fig. 7d). We propose that Mce1 complexes containing either Mce1A or MSMEG_6540
209 may have distinct substrate specificities, perhaps advantageous for an environmental microorganism like
210 *M. smegmatis*.

211 Despite the fact that there are known ABC transporters with heterodimeric TMDs, it has not been
212 appreciated that such asymmetry can give rise to major differences in affinity between each TMD and NBD
213 pair—in the case of the Mce1 transporter, the NBD dimer may be predominantly recruited by YrbE1B (Fig.
214 3c). This might be applicable to other ABC transporters with heterodimeric TMDs since TMD-NBD
215 interfaces of different areas were also observed within some of them (Supplementary Table 2). That TMD-
216 NBD association in the Mce1 transporter relies on the YrbE1B-MceG interaction offers a compelling reason
217 why the negative regulator Mce1N also selectively binds YrbE1B (Fig. 1c, Supplementary Fig. 6a and b).
218 Based on our modeling and biochemical data (Fig. 4a and d), the cytoplasmic domain of Mce1N likely

219 interacts with YrbE1B extensively at a short helix between the latter's N-terminal amphipathic interface
220 helix and TM1. This short helix is nominally a part of TM1 but is presented at an angle due to a kink
221 introduced by a flexible loop within TM1. Remarkably, this structural feature may be exclusively conserved
222 across YrbEBs, but not YrbEAs (Supplementary Fig. 8). This raises an interesting possibility that beyond
223 the most conserved Mce1 complex, Mce1N may also regulate additional Mce systems by binding to the
224 corresponding YrbEB, perhaps providing a way to redistribute MceG among all Mce systems.

225 The discovery of a negative regulator that competes with the NBD for binding to the TMDs may be
226 unique to Mce complexes, as known regulatory mechanisms for ABC transporters typically involve
227 modulation of ATPase activity instead of removing the NBD from the complex[19,33–37]. How and when the
228 Mce1 complex is modulated would directly depend on the levels of Mce1N (Fig. 6), which is highly
229 conserved across the *Mycobacterium* genus (present in both fast- and slow-growing, pathogenic and non-
230 pathogenic species). We note that *mce1N* may be in an operon together with four upstream essential genes
231 involved in porphyrin biosynthesis (*hemACDB*). Porphyrin biosynthesis has been reported to increase,
232 suggesting possible up-regulation of Mce1N (MSMEG_0959), when *M. smegmatis* cells enter dormancy[38].
233 In this situation, negative regulation by Mce1N might be a strategy that cells use to inhibit some Mce
234 complexes to conserve ATP. Alternatively, Mce1N levels may correlate with the need for lipid uptake.
235 Outside the host, where fatty acid substrates may be scarce, it might be preferable for mycobacterial cells
236 to keep the Mce1 system in a routinely OFF state and avoid futile ATP hydrolysis. During infection,
237 however, cells may require a fully active Mce1 complex to utilize host fatty acids. We do not yet know of
238 any environment-dependent regulation of Mce1N. However, it is noteworthy that in *M. leprae*, which
239 possesses Mce1 as the only Mce system[6], Mce1N (ML2418) lacks the C-terminal cytoplasmic domain
240 (Supplementary Fig. 5b) and is likely non-functional. Combined with the fact that *mce1R*, the gene
241 encoding the transcriptional repressor of the *mce1* operon (Supplementary Fig. 1), is absent in *M. leprae*,
242 the pathogen may have lost its ability to down-regulate the Mce1 system, which can facilitate constitutive
243 fatty acid uptake during its obligate parasitic life cycle.

244 We have uncovered a new regulatory mechanism for Mce1 (Fig. 6), and potentially other Mce systems,
245 which may have implications for how mycobacterial cells coordinate lipid uptake processes. Despite the
246 presence of a transcriptional regulator for some *mce* operons (Supplementary Fig. 1), all Mce transporters

247 apparently share the same ATPase MceG[22]. This indicates that mycobacterial cells have the ability to
248 modulate the levels of each complex, yet adjust their activities simultaneously. In the same vein, we
249 speculate that Mce1N could also be a shared negative regulator to counter MceG binding/activation, and
250 primarily functions to deactivate all Mce complexes simultaneously. Whether Mce1N has preferences for
251 specific Mce systems remains to be examined. Nevertheless, it likely contributes significantly to the overall
252 regulation towards maintaining a balanced metabolic flux of different lipid substrates required for
253 mycobacterial survival[11,39], which may involve other yet-to-be-identified uptake transporters beyond Mce
254 systems[40].
255

256 **Methods**

257 **Plasmid construction**

258 Plasmids used in this study were constructed by traditional ligation or Gibson assembly, with mutations
259 introduced by site-directed mutagensis if applicable. Primers used for constructing the plasmids are listed
260 in Supplementary Table 6. Backbone plasmids were digested with relevant restriction enzymes (New
261 England Biolabs). Desired DNA fragments to be inserted were amplified by PCR. For traditional ligation,
262 the insert was digested with the same restriction enzymes as the backbone and ligated with the backbone
263 using T4 DNA ligase (New England Biolabs). For Gibson assembly, desired DNA fragments were inserted
264 into linearized backbones using ClonExpress Ultra One Step Cloning Kit (Vazyme). For site-directed
265 mutagenesis, mutations were introduced to the plasmid using PCR with the original plasmid as the template
266 and primers containing expected changes.
267

268 **Construction of *M. smegmatis* knock-out strains**

269 *M. smegmatis* strains used in this study are listed in Supplementary Table 3. The knockout strains were
270 constructed by two-step homologous recombination as reported previously[41]. Briefly, a suicide plasmid
271 pYUB854 with no replication origin and a *hygR* cassette was used as the backbone for insertion of two
272 flanking regions of the target gene side by side, and a *lacZ-sacB* cassette for blue-white screening and
273 negative selection on sucrose. The plasmid was electroporated at 2250 V using Eporator (Eppendorf) into
274 *M. smegmatis* mc^2155 electrocompetent cells, which were subsequently plated on LB plates containing 50

275 μg/mL hygromycin and 20 μg/mL 5-bromo-4-chloro-3-indolyl-β-D-galactopyranoside (X-gal). The plate
276 was incubated at 37 ºC for 5–7 days to allow the growth of first cross-over cells (those forming blue colonies
277 on the plate). Cells harboring the first cross-over at the targeted site were grown in Middlebrook 7H9 broth
278 containing 0.5% glycerol and 0.05% tyloxapol and spread onto LB plates containing 20 μg/mL X-gal and
279 5% sucrose. The plate was again incubated at 37 ºC for 4 days to allow the growth of second cross-overs
280 (those forming whitish-yellow colonies on the plate). Correct gene deletion mutants were screened by PCR
281 and Sanger sequencing (Bio Basic Asia Pacific, Singapore) among the second cross-overs.
282

283 **Pull-down assay in *M. smegmatis***

284 Plasmids used in this study for protein expression in *M. smegmatis* are listed in Supplementary Table
285 4. pJEB402 or pMV306hsp vectors carrying genes of interest were transformed into *M. smegmatis* cells by
286 electroporation. The cells were grown in 750 mL tryptic soy broth (TSB) supplemented with 0.05% Tween
287 80 to stationary phase (OD_{600} ~5) and harvested by centrifugation at 4,800 xg for 10 min. Harvested cells
288 were resuspended in cold 20 mL TBS (Tris-buffered saline, 20 mM Tris-HCl pH 8.0, 150 mM NaCl)
289 containing 100 μg/mL lysozyme, 100 μM phenylmethylsulfonyl fluoride, and 50 μg/mL DNase I, and lysed
290 by two passages through a French Press (GlenMills) at 18,000 psi. The resulting suspension was centrifuged
291 at 4,800 xg for 4 min to remove unbroken cells. The supernatant containing the cell lysate was subjected to
292 centrifugation at 95,000 xg for 45 min. The pelleted membrane was resuspended in 5 mL extraction buffer
293 (TBS pH 8.0 containing 5 mM $MgCl_2$, 10% glycerol, 5 mM imidazole, and 1% n-dodecyl-β-D-maltoside
294 (DDM)) and extracted on ice with gentle shaking for 2 h. The suspension was subjected to a second round
295 of centrifugation at 89,000 xg for 45 min. The supernatant was loaded onto 100 μL TALON metal affinity
296 resin (Takara Bio) pre-equilibrated with TBS pH 8.0 containing 10 mM imidazole. The mixture was allowed
297 to drain by gravity and the filtrate was loaded back to the column and drained again. The resin was washed
298 with 500 μL washing buffer (20 mM Tris-HCl pH 8.0, 300 mM NaCl, 5 mM $MgCl_2$, 10% glycerol, 8 mM
299 imidazole, and 0.05% DDM) for ten times and subsequently eluted with 100 μL elution buffer (TBS pH 8.0
300 containing 5 mM $MgCl_2$, 10% glycerol, 200 mM imidazole, and 0.05% DDM) for four times. The eluate
301 was concentrated using an Amicon Ultra 10 kDa centrifugal filter (MilliporeSigma) and kept for further
302 SDS-PAGE analysis. Protein gel sections and bands to be identified were sent to Taplin Biological Mass

303 Spectrometry Facility, Harvard Medical School (Boston, MA) for capillary LC-MS/MS analysis.

304

305 **Protein purification from *E. coli***

306 Plasmids used in this study for protein expression in *E. coli* are listed in Supplementary Table 5. *E. coli*
307 BL21(λDE3) cells were used as the host strain. Cells were grown to OD_{600} = 0.6 in 1.5 L LB broth, before
308 1 mM IPTG was added to induce expression of the proteins for 2 h. The cells were harvest by centrifugation
309 at 4,800 xg for 10 min. Harvested cells were resuspended in cold 20 mL TBS (Tris-buffered saline, 20 mM
310 Tris-HCl pH 8.0, 150 mM NaCl) containing 100 µg/mL lysozyme, 100 µM phenylmethylsulfonyl fluoride,
311 and 50 µg/mL DNase I, and lysed by two passages through a French Press at 18,000 psi. The resulting
312 suspension was centrifuged at 4,800 xg for 4 min to remove unbroken cells. The supernatant containing the
313 cell lysate was subjected to centrifugation at 95,000 xg for 45 min. The pelleted membrane was resuspended
314 in the 5 mL extraction buffer (TBS pH 8.0 containing 5 mM $MgCl_2$, 10% glycerol, 5 mM imidazole, and
315 1% DDM) and extracted on ice with gentle shaking for 2 h. The suspension was subjected to a second round
316 of centrifugation at 89,000 xg for 45 min. The supernatant was loaded onto TALON metal affinity resin
317 (Takara Bio) pre-equilibrated with TBS pH 8.0 containing 10 mM imidazole. The mixture was allowed to
318 drain by gravity and the filtrate was loaded back to the column and drained again. The resin was washed
319 10 times with the washing buffer (20 mM Tris-HCl pH 8.0, 300 mM NaCl, 5 mM $MgCl_2$, 10% glycerol, 8
320 mM imidazole, and 0.05% DDM) and subsequently eluted with the elution buffer (TBS pH 8.0 containing
321 5 mM $MgCl_2$, 10% glycerol, 200 mM imidazole, and 0.05% DDM). The eluate was concentrated using an
322 Amicon Ultra 10 kDa centrifugal filter (MilliporeSigma) and subjected to SDS-PAGE analysis. YrbE1A/B-
323 MceG and YrbE1A/B-$MceG_{K43A}$ were further purified and analyzed by SEC (AKTA, GE Healthcare) at 4
324 ºC on a pre-packed Superdex Increase 200 10/300 GL column (Cytiva). TBS pH 8.0 containing 5 mM
325 $MgCl_2$, 10% glycerol, and 0.05% DDM was used as the eluent. Fractions corresponding to the peaks of our
326 interest were concentrated and subjected to SDS-PAGE analysis.

327

328 **SDS-PAGE and Western Blotting**

329 Protein samples were mixed with Laemmli buffer and analyzed by Tris-glycine SDS-PAGE. The gel
330 was visualized by InstantBlue Coomassie Blue Stain (Abcam) or subjected to Western blotting. For the

331 latter, the proteins on the gel were transferred to a polyvinylidene fluoride membrane using a Transblot SD
332 semi-dry transfer system (BioRad) at 25V for 30 min. The membrane was blocked in 1x casein blocking
333 buffer for at least 1 h. For detection of His-tagged proteins, a conjugate of mouse monoclonal penta-His
334 antibody and horseradish peroxidase (Qiagen) was used. For detection of FLAG-tagged proteins, a
335 conjugate of mouse monoclonal FLAG-antibody and horseradish peroxidase (MilliporeSigma) was used.
336 To visualize the blots, Luminata Forte Western HRP Substrate (MilliporeSigma) was applied to the
337 membrane.
338
339 **Disulfide bond analysis**
340 His_6-YrbE1B and MSMEG_0959-FLAG were over-expressed in *E. coli* BL21(λDE3) cells harboring
341 pET28b*his*$_6$*-yrbE1B* and pCDFduet*MSMEG_0959-FLAG*, with site-specific cysteine substitutions. The
342 cells were grown to OD_{600} = 0.6 in LB broth, before 1 mM IPTG was added to induce expression of the
343 proteins for 2 h. The cells were harvest by centrifugation at 4,000 xg for 3 min. The pellets were resuspended
344 in 2x Laemmeli buffer with (for reducing conditions) or without (for non-reducing conditions) 10% β-
345 mecaptoethanol. The samples were centrifuged at 21,000 xg for 10 min before being subjected to SDS-
346 PAGE and immunoblot analyses.
347
348 **Determination of cell growth in different media**
349 *M. smegmatis* cells were grown in Middlebrook 7H9 broth containing 0.5% glycerol and 0.05%
350 tyloxapol to an OD_{600} around 2. The cells were subcultured into the same 7H9 medium or into Sauton's
351 medium (0.5 g/L K_2HPO_4, 0.25 g/L $MgSO_4$, 2 g/L citric acid, 0.4 g/L L-asparagine, 0.05 g/L ferric
352 ammonium citrate, 5 g/L fatty acid-free bovine serum albumin, 0.05% tyloxapol, pH 7.0) containing
353 palmitic acid as the sole carbon source. The starting OD_{600} for the subculture was 0.001 for the 7H9 medium
354 and 0.0001 for the Sauton's medium. To prepare the Sauton's medium, palmitic acid was dissolved in 0.1
355 M NaOH, heated to 80 ºC and added into the medium with constant stirring to a final concentration of 300
356 μM. The cultures were incubated at 37 ºC with 200 rpm shaking. Growth of the cells were monitored at
357 specified time points using a UV-Vis spectrophotometer at 600 nm.
358

359 **Palmitic acid uptake assay**

360 The palmitic acid uptake assay was adapted from the one used in ref. [11]. *M. smegmatis* cells were grown
361 in the Middlebrook 7H9-glycerol-tyloxapol medium until the stationary phase and sub-cultured into
362 Sauton's medium with palmitate as the carbon source or TSB for cells over-expressing Mce1Ns. Stationary-
363 phase cells (OD_{600} ~0.4 for cells grown in Sauton and ~5 for those in TSB) were pelleted by centrifugation
364 at 3,000 xg for 4 min and resuspended in 1x phosphate-buffered saline (PBS) supplemented with 0.05%
365 Triton X-100 and 0.1% fatty acid-free bovine serum albumin (BSA) yielding a final OD_{600} of 0.8. [^{14}C]-
366 palmitic acid (Perkin Elmer) was added to a final activity concentration of 0.2 µCi/mL. The cells were
367 incubated at 37 ºC with 200 rpm shaking. Cells were harvested at different time points (5, 15, 30, 45 min)
368 by centrifugation at 5,000 xg for 1 min from 300 µL suspension and washed once with ice-cold PBS
369 containing Triton X-100 and BSA. The cells were finally resuspended in the same buffer and aliquoted into
370 three plastic scintillation vials for counting using a MicroBeta2 microplate counter (Perkin Elmer).

371

372 **Enzyme-coupled ATPase assay**

373 ATP hydrolytic activity was measured using an NADH-coupled assay[42] adapted for plate readers[43], as
374 previously described[19]. Each 50 µL reaction is made up of 20 mM Tris-HCl pH 8.0, 150 mM NaCl, 5 mM
375 $MgCl_2$,10% glycerol, 0.05% DDM, 200 mM NADH (MilliporeSigma), 20 U/mL lactic dehydrogenase
376 (MilliporeSigma), 100 U/mL pyruvate kinase (MilliporeSigma), 0.5 mM phosphoenolpyruvate
377 (MilliporeSigma) and various ATP (MilliporeSigma) concentrations. Protein complexes were added to a
378 final concentration of 0.1 µM. Fluorescence emission at 340 nm from the reaction mixture was monitored
379 at 37°C with 15 s intervals using a Biotek Synergy H1 microplate reader equipped with Biotek Gen5
380 software (Agilent). A linear fit was performed for the measured fluorescence within 10 min reaction time
381 to obtain the rate of decrease in NADH fluorescence, which was converted to ATP hydrolysis rates using a
382 standard curve obtained with known ADP concentrations. The assay for each sample was performed in
383 technical triplicates and the data were fit to the built-in Hill equation in OriginPro 2018b.

384

385 **Bioinformatic and structural analyses**

386 Topological prediction for MSMEG_0959 was done using the CCTOP server (http://cctop.ttk.hu/).

387 Sequence alignment of proteins was done using pairwise (EMBOSS needle) or multiple sequence alignment
388 (Clustal Omega) tools provided by EMBL-EBI (https://www.ebi.ac.uk/services). Structural prediction for
389 YrbE1A/B-MceG, YrbEA/Bs-MSMEG_0959 was done using ColabFold[28] on the Colaboratory server
390 (Google). Prediction for Mce hexamers was done using the AlphaFold multimer tool on the COSMIC[2]
391 platform[26,30]. For both predictions, no template information was used and Amber was used for relaxing the
392 predicted models. Other settings were kept as default. Visualization of structures and overlay of structural
393 models were performed using PyMOL 2.3.0. Interface analysis was performed using ChimeraX 1.4.
394

395 **References**

396 1. World Health Organization. Global Tuberculosis Report 2022.
397 https://www.who.int/publications/i/item/9789240061729 (2022).
398 2. Houben, R. M. & Dodd, P. J. The global burden of latent tuberculosis infection: a re-estimation using
399 mathematical modelling. *PLoS Med*. **13**, e1002152 (2016).
400 3. Chai, Q., Zhang, Y. & Liu, C. H. *Mycobacterium tuberculosis*: an adaptable pathogen associated with
401 multiple human diseases. *Front*. *Cell*. *Infect*. *Microbiol*. **8**, 158 (2018).
402 4. Forrellad, M. A. et al. Virulence factors of the *Mycobacterium tuberculosis* complex. *Virulence* **4**, 3-66
403 (2013).
404 5. Klepp, L. I., García, J. S. y & Bigi, F. Mycobacterial MCE proteins as transporters that control lipid
405 homeostasis of the cell wall. *Tuberculosis (Edinb)* **132**, 102162 (2022).
406 6. Casali, N. & Riley, L. W. A phylogenomic analysis of the *Actinomycetales mce* operons. *BMC*
407 *Genomics* **8**, 60 (2007).
408 7. Shimono, N. et al. Hypervirulent mutant of *Mycobacterium tuberculosis* resulting from disruption of
409 the *mce1* operon. *Proc*. *Natl*. *Acad*. *Sci*. *U*. *S*. *A*. **100**, 15918-15923 (2003).
410 8. Gioffré, A. et al. Mutation in *mce* operons attenuates *Mycobacterium tuberculosis* virulence. *Microbes*
411 *Infect*. **7**, 325-334 (2005).
412 9. Pandey, A. K. & Sassetti, C. M. Mycobacterial persistence requires the utilization of host cholesterol.
413 *Proc*. *Natl*. *Acad*. *Sci*. *U*. *S*. *A*. **105**, 4376-4380 (2008).
414 10. Senaratne, R. H. et al. *Mycobacterium tuberculosis* strains disrupted in *mce3* and *mce4* operons are

415 attenuated in mice. *J. Med. Microbiol.* **57**, 164-170 (2008).
416 11. Nazarova, E. V et al. Rv3723/LucA coordinates fatty acid and cholesterol uptake in *Mycobacterium*
417 *tuberculosis*. *eLife* **6** (2017).
418 12. Rank, L., Herring, L. E. & Braunstein, M. Evidence for the mycobacterial Mce4 transporter being a
419 multiprotein complex. *J. Bacteriol.* **203**, e00685-00620 (2021).
420 13. Casali, N., White, A. M. & Riley, L. W. Regulation of the *Mycobacterium tuberculosis mce1* operon. *J.*
421 *Bacteriol.* **188**, 441-449 (2006).
422 14. Santangelo, M. P. et al. Study of the role of Mce3R on the transcription of *mce* genes of *Mycobacterium*
423 *tuberculosis*. *BMC Microbiol.* **8**, 38 (2008).
424 15. Forrellad, M. A. et al. Role of the Mce1 transporter in the lipid homeostasis of *Mycobacterium*
425 *tuberculosis*. *Tuberculosis (Edinb)* **94**, 170-177 (2014).
426 16. Malinverni, J. C. & Silhavy, T. J. An ABC transport system that maintains lipid asymmetry in the Gram-
427 negative outer membrane. *Proc. Natl. Acad. Sci. U. S. A.* **106**, 8009-8014 (2009).
428 17. Tang, X. et al. Structural insights into outer membrane asymmetry maintenance in Gram-negative
429 bacteria by MlaFEDB. *Nat. Struct. Mol. Biol.* **28**, 81-91 (2021).
430 18. Low, W.-Y., Thong, S. & Chng, S.-S. ATP disrupts lipid-binding equilibrium to drive retrograde
431 transport critical for bacterial outer membrane asymmetry. *Proc. Natl. Acad. Sci. U. S. A.* **118** (2021).
432 19. Thong, S. et al. Defining key roles for auxiliary proteins in an ABC transporter that maintains bacterial
433 outer membrane lipid asymmetry. *eLife* **5** (2016).
434 20. Ekiert, D. C. et al. Architectures of Lipid Transport Systems for the Bacterial Outer Membrane. *Cell*
435 **169**, 273-285 e217 (2017).
436 21. Joshi, S. M. et al. Characterization of mycobacterial virulence genes through genetic interaction
437 mapping. *Proc Natl Acad Sci U S A* **103**, 11760-11765 (2006).
438 22. Garcia-Fernández, J., Papavinasasundaram, K., Galán, B., Sassetti, C. M. & García, J. L. Unravelling
439 the pleiotropic role of the MceG ATPase in *Mycobacterium smegmatis*. *Environ. Microbiol.* **19**, 2564-
440 2576 (2017).
441 23. Liu, C., Ma, J., Wang, J., Wang, H. & Zhang, L. Cryo-EM structure of a bacterial lipid transporter YebT.
442 *J. Mol. Biol.* **432**, 1008-1019 (2020).

443 24. Isom, G. L. et al. LetB structure reveals a tunnel for lipid transport across the bacterial envelope. *Cell*
444 **181**, 653-664 (2020).
445 25. Perkowski, E. F. et al. An orphaned Mce-associated membrane protein of *Mycobacterium tuberculosis*
446 is a virulence factor that stabilizes Mce transporters. *Mol. Microbiol.* **100**, 90-107 (2016).
447 26. Evans, R. et al. Protein complex prediction with AlphaFold-Multimer. Preprint at
448 https://www.biorxiv.org/content/10.1101/2021.10.04.463034v2 (2022).
449 27. Jumper, J. et al. Highly accurate protein structure prediction with AlphaFold. *Nature* **596**, 583-589
450 (2021).
451 28. Mirdita, M. et al. ColabFold: making protein folding accessible to all. *Nat. Methods* **19**, 679-682 (2022).
452 29. Zhou, C. et al. Structural insight into phospholipid transport by the MlaFEBD complex from *P.*
453 *aeruginosa*. *J. Mol. Biol.* **433**, 166986 (2021).
454 30. Cianfrocco, M. A., Wong, M., Youn, C., Wagner, R. & Leschziner, A. E. COSMIC²: A science gateway
455 for cryo-electron microscopy structure determination. *Proceedings of the Practice and Experience in*
456 *Advanced Research Computing 2017 on Sustainability, Success and Impact* 1-5 (2017).
457 31. Asthana, P. et al. Structural insights into the substrate-binding proteins Mce1A and Mce4A from
458 *Mycobacterium tuberculosis*. *IUCrJ* **8**, 757-774 (2021).
459 32. Chen, J. *et al*. Structure of an endogenous mycobacterial MCE lipid transporter. Preprint at
460 https://www.biorxiv.org/content/10.1101/2022.12.08.519548v2 (2022).
461 33. Crawford, R. R., Potukuchi, P. K., Schuetz, E. G. & Schuetz, J. D., Beyond competitive inhibition:
462 regulation of ABC transporters by kinases and protein-protein interactions as potential mechanisms of
463 drug-drug interactions. *Drug Metab. Dispos.* **46**, 567-580 (2018).
464 34. Kadaba, N. S., Kaiser, J. T., Johnson, E., Lee, A. & Rees, D. C. The high-affinity *E. coli* methionine
465 ABC transporter: structure and allosteric regulation. *Science* **321**, 250-253 (2008).
466 35. Gerber, S., Comellas-Bigler, M., Goetz, B. A. & Locher, K. P. Structural basis of trans-inhibition in a
467 molybdate/tungstate ABC transporter. *Science* **321**, 246-250.
468 36. Chen, S., Oldham, M. L., Davidson, A. L. & Chen, J. Carbon catabolite repression of the maltose
469 transporter revealed by X-ray crystallography. *Nature* **499**, 364-368 (2013).
470 37. Ko, S. B. et al. Gating of CFTR by the STAS domain of SLC26 transporters. *Nat. Cell. Biol.* **6**, 343-

350 (2004).

38. Nikitushkin, V. D. et al. The main pigment of the dormant *Mycobacterium smegmatis* is porphyrin. *FEMS Microbiol*. *Lett*. **363** (2016).

39. Lee, W., VanderVen, B. C., Fahey, R. J. & Russell, D. G. Intracellular *Mycobacterium tuberculosis* exploits host-derived fatty acids to limit metabolic stress. *J*. *Biol*. *Chem*. **288**, 6788-6800 (2013).

40. Martin, A. & J. Daniel. The ABC transporter Rv1272c of *Mycobacterium tuberculosis* enhances the import of long-chain fatty acids in *Escherichia coli*. *Biochem*. *Biophys*. *Res*. *Commun*. **496**, 667-672 (2018).

41. Parish, T. & Stoker, N. G. Use of a flexible cassette method to generate a double unmarked *Mycobacterium tuberculosis tlyA plcABC* mutant by gene replacement. *Microbiology* **146**, 1969-1975 (2000).

42. Nørby, J. G. Coupled assay of Na^+, K^+-ATPase activity. *Methods Enzymol*. **156**, 116–119 (1988).

43. Kiianitsa, K., Solinger, J. A. & Heyer, W.-D. NADH-coupled microplate photometric assay for kinetic studies of ATP-hydrolyzing enzymes with low and high specific activities. *Anal*. *Biochem*. **321**, 266-271 (2003).

Data availability

All data are available in the main text or supplementary materials of this manuscript.

Acknowledgements

We thank Jia Fu Erh and Wei Shen Ho (National University of Singapore) for constructing plasmids and early affinity purification attempts. We are grateful to Beijing Genomics Institute (BGI) Research for providing DNA synthesis and assembly support. We thank Ross Tomaino (Taplin MS facility, Harvard Medical School) for help with protein identification. This work was supported by Singapore Ministry of Education Academic Research Fund Tier 2 grants MOE2019-T2-1-128 and MOE000116 (S.-S.C).

Author contributions

Y.C. and S.-S.C. conceptualized the study, designed the experiments, analyzed the data, and wrote the manuscript. Y.C. performed the experimental studies. Y.W. performed the disulfide crosslinking experiment. S.-S.C. supervised the study.

Competing interests

The authors declare that they have no competing interests.

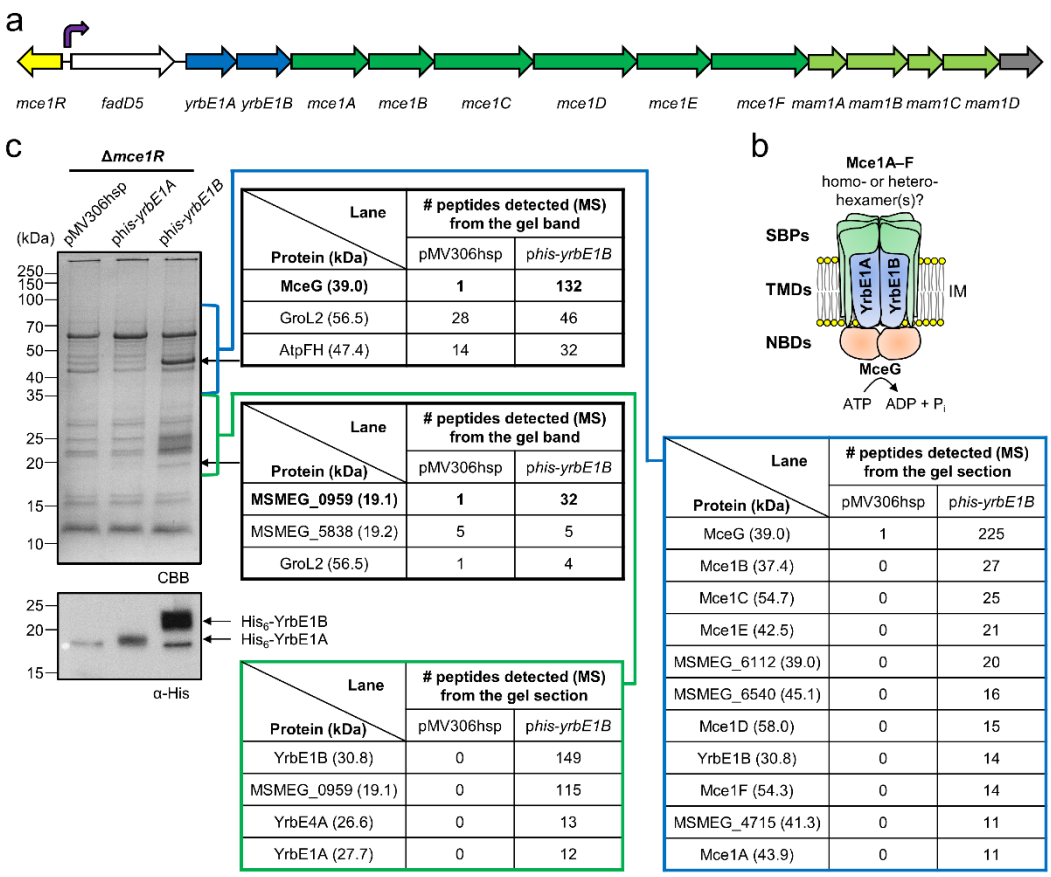

Protein (kDa) \ Lane	# peptides detected (MS) from the gel band	
	pMV306hsp	*phis-yrbE1B*
MceG (39.0)	**1**	**132**
GroL2 (56.5)	28	46
AtpFH (47.4)	14	32

Protein (kDa) \ Lane	# peptides detected (MS) from the gel band	
	pMV306hsp	*phis-yrbE1B*
MSMEG_0959 (19.1)	**1**	**32**
MSMEG_5838 (19.2)	5	5
GroL2 (56.5)	1	4

Protein (kDa) \ Lane	# peptides detected (MS) from the gel section	
	pMV306hsp	*phis-yrbE1B*
YrbE1B (30.8)	0	149
MSMEG_0959 (19.1)	0	115
YrbE4A (26.6)	0	13
YrbE1A (27.7)	0	12

Protein (kDa) \ Lane	# peptides detected (MS) from the gel section	
	pMV306hsp	*phis-yrbE1B*
MceG (39.0)	1	225
Mce1B (37.4)	0	27
Mce1C (54.7)	0	25
Mce1E (42.5)	0	21
MSMEG_6112 (39.0)	0	20
MSMEG_6540 (45.1)	0	16
Mce1D (58.0)	0	15
YrbE1B (30.8)	0	14
Mce1F (54.3)	0	14
MSMEG_4715 (41.3)	0	11
Mce1A (43.9)	0	11

Figure 1. Affinity purification with His$_6$-YrbE1B defines the composition of Mce1 complexes. a A schematic representation of the *mce1* genetic loci in *M. smegmatis*. Each straight arrow represents an individual gene. Lengths of the arrows are scaled to the lengths of the genes. The gene encoding a putative transcriptional regulator of the *mce1* operon is colored in *yellow*. A gene encoding a putative acyl-CoA synthase is colored in white. *yrbE* genes are colored in *blue*, *mce* genes *dark green*, *mam* genes *light green*, and unrelated genes *grey*. The promoter position of the *mce1* operon is annotated with a turning arrow in *purple*. **b** A basic model of the putative Mce1 complex based on current knowledge. SBP (Mce1A–F), substrate-binding protein; TMD (YrbE1A/B), transmembrane domain; NBD (MceG), nucleotide-binding domain; IM, inner membrane. **c** SDS-PAGE and α-His immunoblot analyses of proteins affinity-purified from *M. smegmatis* Δ*mce1R* cells expressing His-tagged YrbE1A (p*his-yrbE1A*) or YrbE1B (p*his-yrbE1B)*. pMV306hsp was used as the empty vector control. For protein identification from gel bands, the top three proteins detected in the p*his-yrbE1B* lane are listed. For protein identification from gel sections (blue: 35–90 kDa, green: 18–35 kDa), proteins with more than ten total peptides detected and significantly enriched in the p*his-yrbE1B* lane are listed. CBB, Coomassie brilliant blue; MS, mass spectrometry.

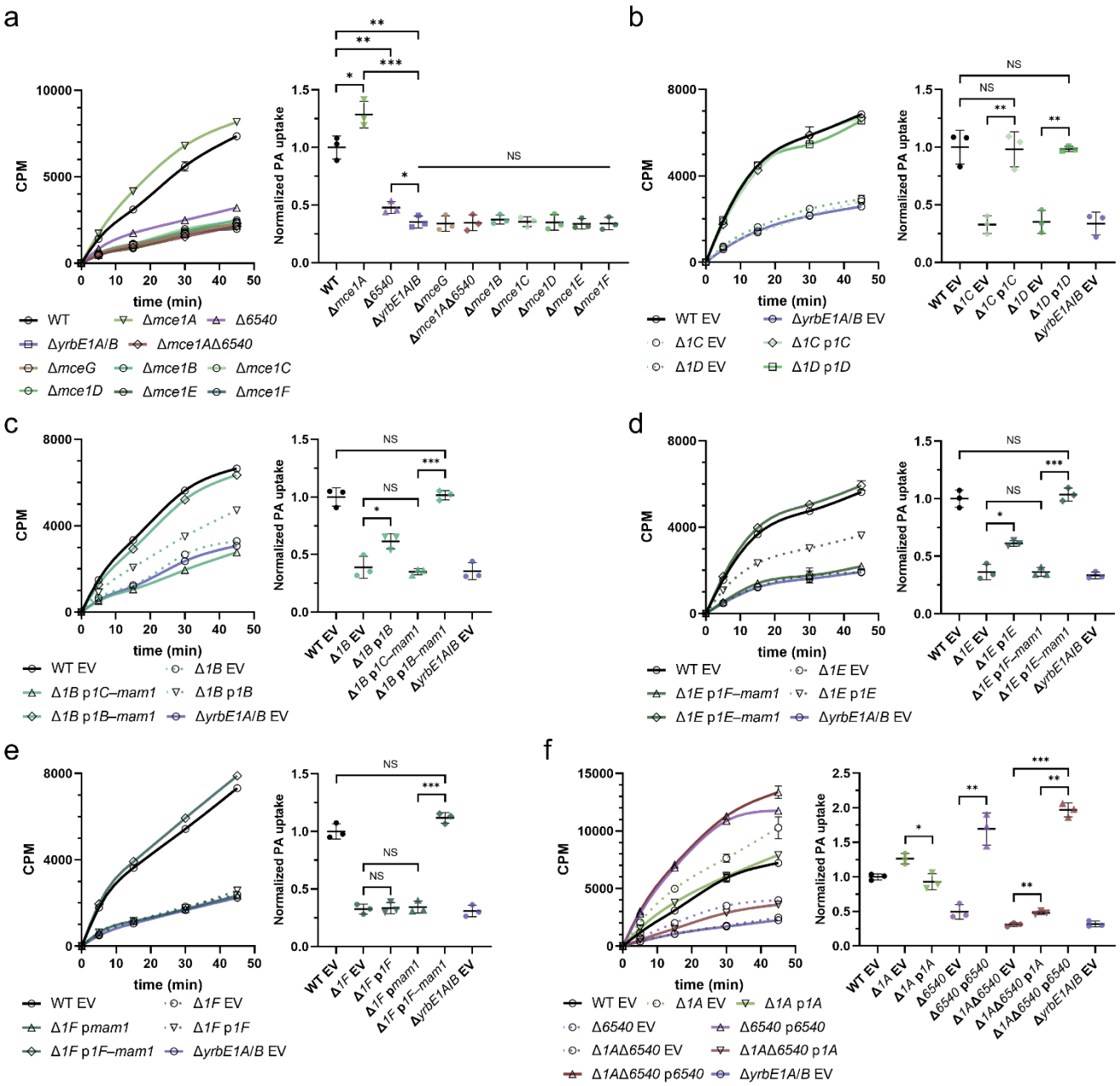

Figure 2. MSMEG_6540 and Mce1A are redundant components that likely form heterohexamers with Mce1B–F in Mce1 complexes. a–f [^{14}C]-palmitic acid uptake profiles and rates of indicated *M. smegmatis* strains. Each uptake profile (*left*) shows accumulated radioactivity counts in cells over time, and is representative of at least three independent experiments. Each data point (mean ± standard deviation) represents results from three *technical* replicates. CPM, count per minute. Uptake rates (*right*) are quantified based on [^{14}C]-palmitic acid levels after 30 min incubation. The uptake of individual strains is normalized to that of wild type (WT) cells or WT cells harboring the empty vector (WT EV). Mean ± standard deviation of three *biological* replicates is shown for each group. Welch's t-test: NS, not significant;

527 * $p<0.05$; ** $p<0.01$; *** $p<0.001$. In **b**–**f**, different strains in **a** are complemented via expression of
528 indicated genes from a plasmid. *MSMEG_6540* and *mce1A–F* genes are annotated as *6540* and *1A–F*
529 respectively. EV, empty vector (pJEB402).

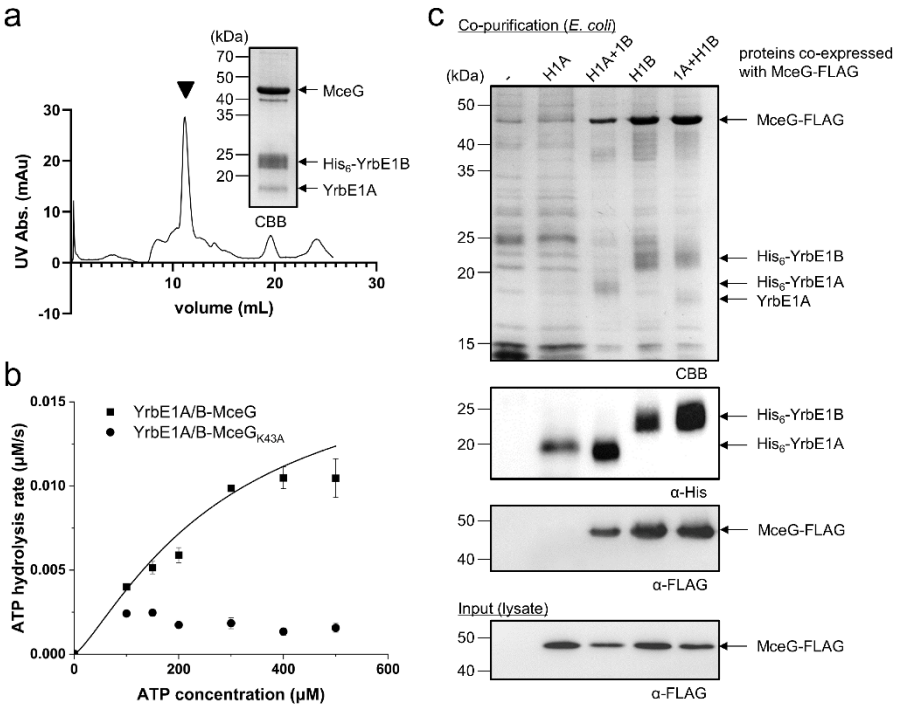

Figure 3. YrbE1A/B-MceG form a stable asymmetric complex with ATPase activity. a Size exclusion chromatographic profile of the purified complex comprising YrbE1A, His_6-YrbE1B and MceG. SDS-PAGE analysis of the peak corresponding to the complex (black arrowhead) is shown. **b** Enzyme-coupled ATPase assay of 0.1 μM YrbE1A/B-MceG and YrbE1A/B-$MceG_{K43A}$ in detergent micelles at 37 ºC. Average ATP hydrolysis rates from three technical triplicates were plotted against ATP concentrations, and fitted to an expanded Michaelis-Menten equation that includes a term for Hill coefficient (n). YrbE1A/B-MceG: $K_m = 284 \pm 311$μM, $k_{cat} = 0.184 \pm 0.125$ μM ATP s^{-1}/μM complex, n = 1.28 ± 0.57. The data for the mutant failed to fit to the equation with significant confidence. Each data point is shown as mean ± standard deviation. **c** SDS-PAGE and α-His/FLAG immunoblot analyses of proteins affinity-purified from *E. coli* cells over-expressing FLAG-tagged MceG together with either His_6-YrbE1A (H1A) with/without YrbE1B (1B) or His_6-YrbE1B (H1B) with/without YrbE1A (1A). CBB, Coomassie brilliant blue.

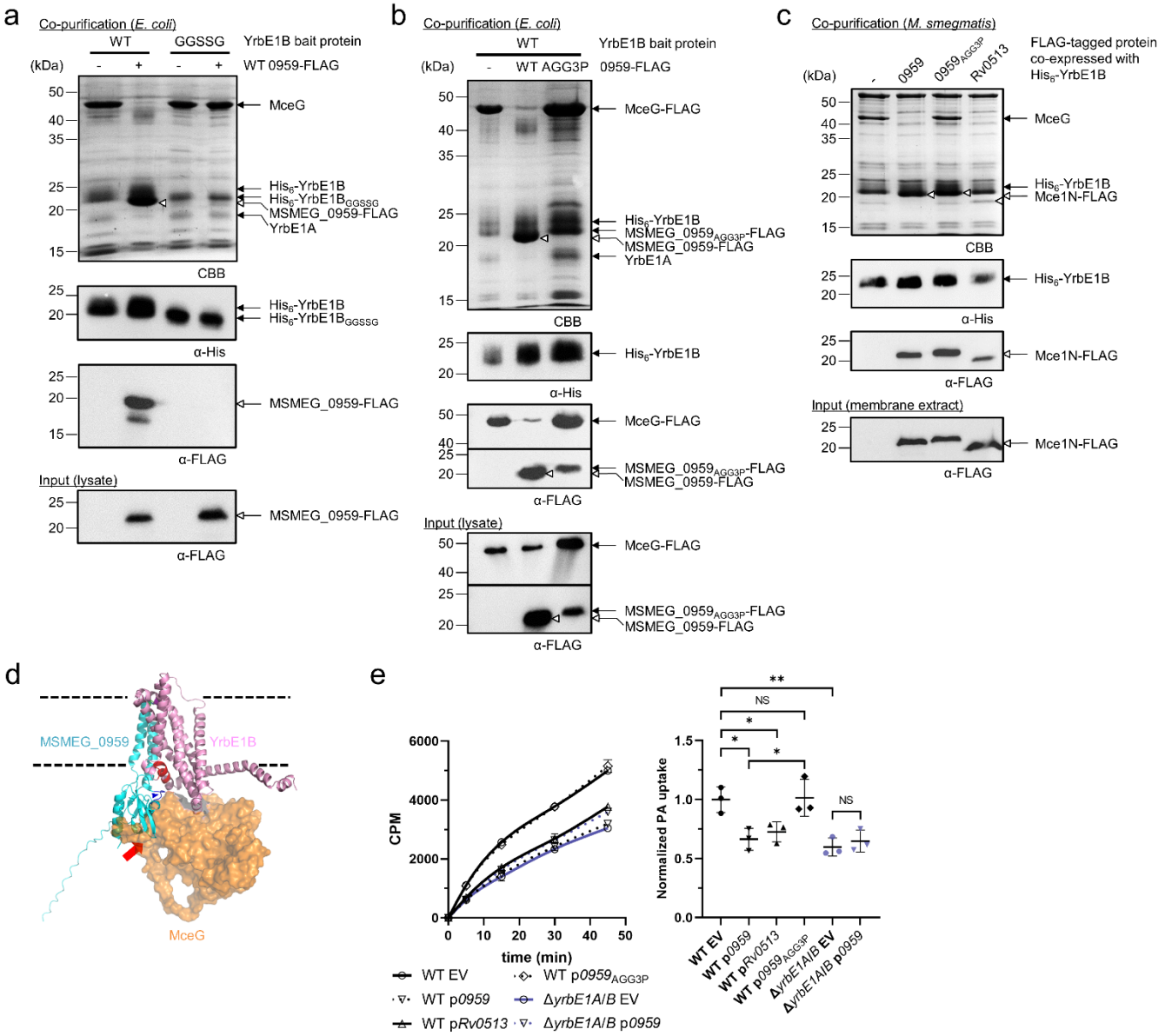

Figure 4. MSMEG_0959 negatively regulates the Mce1 transporter. a SDS-PAGE and α-His/FLAG immunoblot analyses of proteins affinity-purified from *E. coli* cells over-expressing YrbE1A, MceG, and either wild-type His_6-YrbE1B (WT) or the helix-to-loop mutant His_6-YrbE1B (GGSSG), in the presence (+) or absence (-) of MSMEG_0959-FLAG. **b** SDS-PAGE and α-His/FLAG immunoblot analyses of proteins affinity-purified from *E. coli* cells over-expressing YrbE1A, FLAG-tagged MceG, His-tagged YrbE1B together with FLAG-tagged wild type MSMEG_0959 (WT) or the loop-rigidified mutant (AGG3P). **c** SDS-PAGE and α-His/FLAG immunoblot analyses of proteins affinity-purified from *M. smegmatis* cells over-expressing His_6-YrbE1B as the bait protein together with MSMEG_0959, the loop-rigidified mutant (0959_{AGG3P}) or Rv0513 (Mce1N from *M. tuberculosis*). **d** An overlay of AlphaFold2 models of YrbE1B (*pink*)-MceG (*orange* surface) and YrbE1B-MSMEG_0959 (*cyan*). The helix-to-loop

553 mutation of YrbE1B located on the putative short helix at the YrbE1B-MSMEG_0959 interface is
554 highlighted in *red*. The rigidified loop on the MSMEG_0959$_{AGG3P}$ mutant is highlighted in *blue* (with an
555 arrowhead). The steric clash between MceG and MSMEG_0959 is indicated by a *red* arrow. Dashed lines
556 represent arbitrary membrane boundaries based on hydrophobicity of the transmembrane regions. **e** [^{14}C]-
557 palmitic acid uptake profiles and rates of indicated *M. smegmatis* strains over-expressing different Mce1Ns
558 from a plasmid grown in the same condition as in **c**. The uptake profile (*left*) shows accumulated
559 radioactivity counts in cells over time, and is representative of at least three independent experiments. Each
560 data point (mean ± standard deviation) represents results from three *technical* replicates. CPM, count per
561 minute. Uptake rates (*right*) are quantified based on [^{14}C]-palmitic acid levels after 30 min incubation. The
562 uptake of individual strains is normalized to that of WT cells harboring the empty vector (WT EV). Mean
563 ± standard deviation of three *biological* replicates is shown for each group. Welch's t-test: NS, not
564 significant; * $p<0.05$; ** $p<0.01$. EV, empty vector (pMV306hsp); *0959*, *MSMEG_0959*.

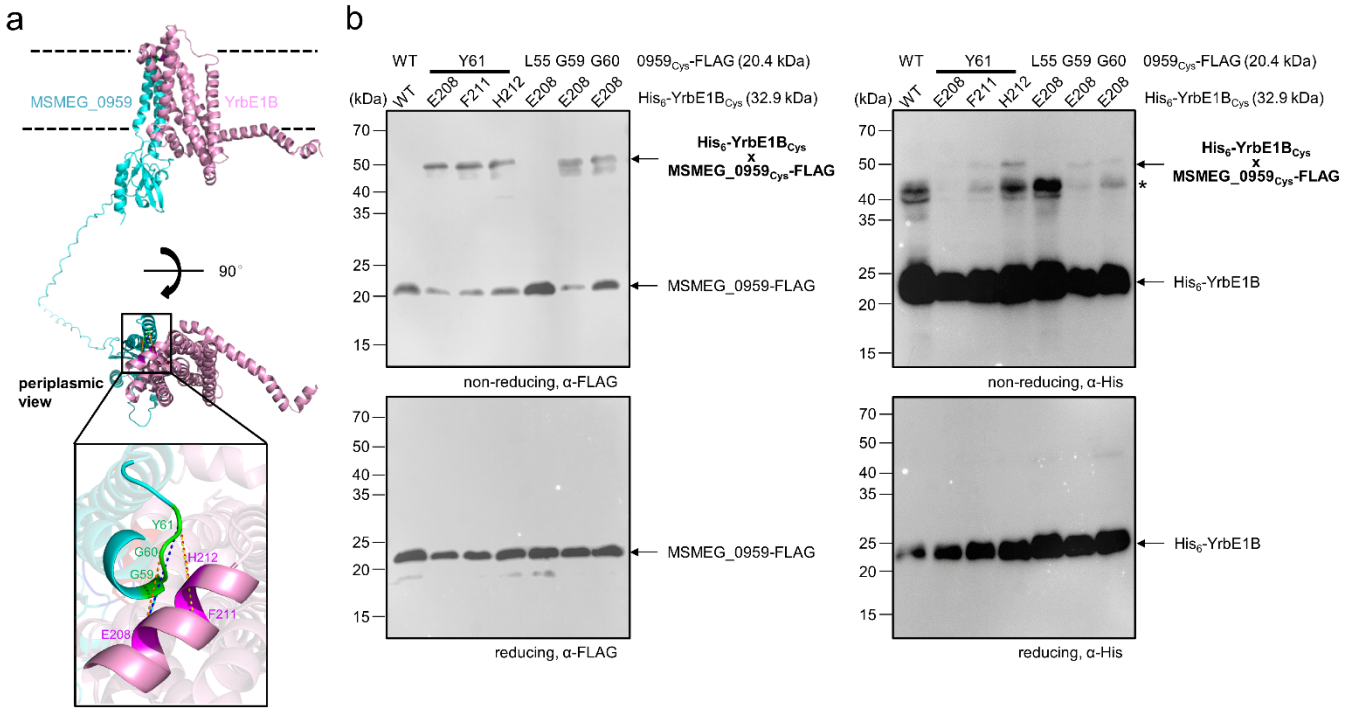

Figure 5. Disulfide crosslinking validates the predicted YrbE1B-MSMEG-0959 model. a A zoomed-in view of contact sites between YrbE1B and MSMEG_0959 revealed by disulfide crosslinks and mapped onto the AlphaFold2 model. Positions on YrbE1B and MSMEG_0959 that allowed disulfide formation between the two proteins (see **b**) are highlighted in *magenta* and *green*, respectively. **b** α-FLAG (*left*) and α-His (*right*) immunoblot analyses showing crosslinking adducts formed, if any, between MSMEG_0959-FLAG and His_6-YrbE1B with cysteines incorporated at indicated sites, when the two proteins were expressed in *E. coli*. Wild type His_6-YrbE1B and MSMEG_0959-FLAG (Lane 1) serve as negative control. The samples were subjected to non-reducing or reducing SDS-PAGE before immunoblotting. A band putatively assigned as His_6-YrbE1B dimers is denoted with an asterisk.

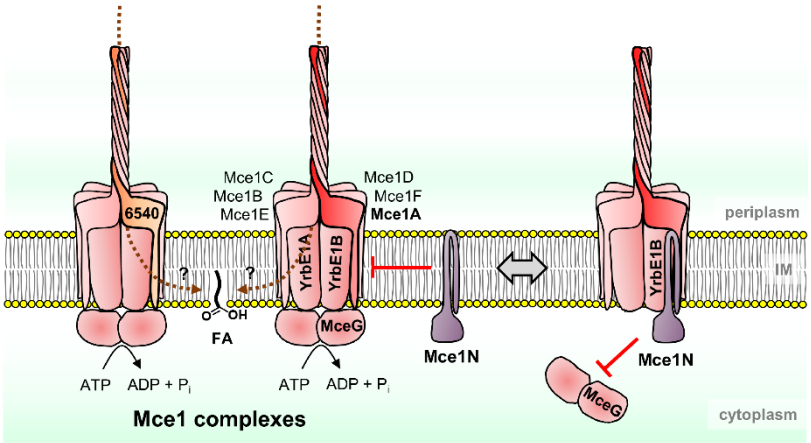

575

576 **Figure 6. A proposed model of Mce1 complexes and their regulation by Mce1N.** Mce1 complexes are
577 ABC transporters for fatty acids, with YrbE1A/B as TMDs, MceG as NBDs, and heterohexameric MCE-
578 domain proteins as SBPs. There are two variants of Mce1 complexes in *M. smegmatis*, each containing
579 MSMEG_6540 or Mce1A in addition to Mce1B–F. The relative order of protomers within heterohexameric
580 SBP complexes is indicated based on the AlphaFold2 models (Supplementary Fig. 7b). Mce1N is a negative
581 regulator of the Mce1 system; it specifically binds to YrbE1B and prevents its interaction with MceG.